*J. Plasma Physics* (2012), *vol.* 78, *part* 4, *pp.* 393–399. © Cambridge University Press 2012
doi:10.1017/S0022377812000220


# High resolution electron beam measurements on the ALPHA-X laser–plasma wakefield accelerator

G. H. WELSH, S. M. WIGGINS, R. C. ISSAC, E. BRUNETTI, G. G. MANAHAN, M. R. ISLAM, S. CIPICCIA, C. ANICULAESEI, B. ERSFELD and D. A. JAROSZYNSKI

Department of Physics, Scottish Universities Physics Alliance, University of Strathclyde, Glasgow, G4 0NG, UK (g.welsh@strath.ac.uk)

(Received 21 October 2011; revised 24 January 2012; accepted 26 January 2012; first published online 27 February 2012)

**Abstract.** The Advanced Laser–Plasma High-Energy Accelerators towards X-rays (ALPHA-X) programme at the University of Strathclyde is developing laser–plasma accelerators for the production of ultra-short high quality electron bunches. Focussing such LWFA bunches into an undulator, for example, requires particular attention to be paid to the emittance, electron bunch duration and energy spread. On the ALPHA-X wakefield accelerator beam line, a high intensity ultra-short pulse from a 30 TW Ti:Sapphire laser is focussed into a helium gas jet to produce femtosecond duration electron bunches in the range of 90–220 MeV. Measurements of the electron energy spectrum, obtained using a high resolution magnetic dipole spectrometer, show electron bunch r.m.s. energy spreads down to 0.5%. A pepper-pot mask is used to obtain transverse emittance measurements of a $128 \pm 3$ MeV mono-energetic electron beam. An average normalized emittance of $\varepsilon_{\mathrm{rms,x,y}} = 2.2 \pm 0.7, 2.3 \pm 0.6$ $\pi$-mm-mrad is measured, which is comparable to that of a conventional radio-frequency accelerator. The best measured emittance of $\varepsilon_{\mathrm{rms,x,}} = 1.1 \pm 0.1$ $\pi$-mm-mrad corresponds to the resolution limit of the detection system. 3D particle-in-cell simulations of the ALPHA-X accelerator partially replicate the generation of low emittance, low energy spread bunches with charge less than 4 pC and gas flow simulations indicate both long density ramps and shock formation in the gas jet nozzle.

## 1. Introduction

Since laser–wakefield accelerators (LWFAs) were first postulated by Tajima and Dawson in 1979 (Tajima and Dawson 1979), the advancement of laser technology has allowed their concept, of harnessing the strong ponderomotive force of a laser beam to excite plasma waves and form wave-like structures (Sprangle et al. 1990) that travel with a velocity close to the speed of light, to become reality. The LWFA now enters a new area of technology where it lends itself well to applications that previously required higher levels of expenditure and large experiment areas associated with conventional radio-frequency (RF) accelerators. The production of high quality electron beams, consisting of mono-energetic (Rechatin et al. 2009; Wiggins et al. 2010), tunable energy (Mangles et al. 2004; Faure et al. 2006; Leemans et al. 2006), low emittance (Fritzler et al. 2004; Brunetti et al. 2010; Sears et al. 2010) and short bunch length (Lundh et al. 2011) is readily achievable using compact, high power laser technology. With further refinement and the inclusion of high peak currents, the LWFA shows great promise as a driver for a compact free electron laser (FEL) (Jaroszynski et al. 2006), and due to the energy range available produces radiation from the visible (Schlenvoigt et al. 2008) and ultra-violet (Fuchs et al. 2009) to the X-ray (Rousse et al. 2004) and gamma-ray (Cipiccia et al. 2011) spectral regions.

Here, we present the compact design utilized in the Advanced Laser–Plasma High-energy Accelerators towards X-rays (ALPHA-X) LWFA. The ALPHA-X beam line has demonstrated the production of suitable electrons for both driving a compact FEL and advancing compact accelerator applications.

## 2. Experimental set-up

The ALPHA-X laser–wakefield accelerator beam line (shown in Fig. 1) at the University of Strathclyde (Jaroszynski et al. 2006) has been used to conduct experiments studying electron beam generation and their associated properties. A high power Ti:Sapphire laser pulse (wavelength = 800 nm, energy = 0.9 J on target, duration = 35 fs) is focussed using a f/18 spherical mirror to a spot size of $\omega_0 = 40\,\mu\mathrm{m}$ ($1/e^2$ diameter), giving a maximum peak intensity $I = 2 \times 10^{18}\,\mathrm{W\,cm^{-2}}$, corresponding to a normalized vector potential $a_0 \approx 1.0$. The laser beam interacts with a 2 mm diameter

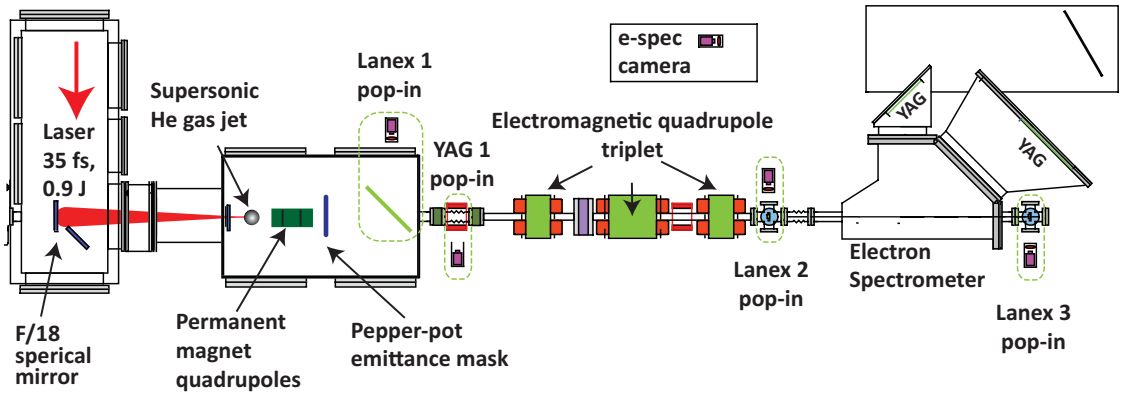


**Figure 1.** (Colour online) Scale diagram of the ALPHA-X experimental beam line.

pulsed supersonic helium gas jet, compressing to a 10 μm diameter relativistic plasma channel with a density of $\sim 1-3\times10^{19}\,\mathrm{cm}^{-3}$ just inside the leading edge of the gas jet.

The intensity of the laser is high enough to allow self-guiding of the laser across the gas jet. For this to occur the critical laser power $P_{\mathrm{cr}}$ must exceed the limit governed by $P_{\mathrm{cr}} \sim 17(\omega/\omega_{\mathrm{p}})^2$ GW (Sun et al. 1987), where $\omega$ and $\omega_{\mathrm{p}}$ are the laser and plasma frequencies, respectively. The ponderomotive force pushes the electrons from the high intensity region. The void created is referred to as the bubble and is analogous with the wake created behind a boat travelling on the surface of water. The size of the bubble can be clearly defined as having a radius $\sqrt{a_0}\lambda_{\mathrm{p}}/\pi$ (Lu et al. 2007) with $\lambda_{\mathrm{p}}$ the plasma wavelength. Depending on the laser parameters and the plasma density profile (and therefore bubble size), a stable operating regime can be obtained. To preserve the high quality of the electron beam careful consideration must be given to optimizing beam transport after acceleration. Removable Lanex and Ce:YAG screens are strategically placed along the beam line (Fig. 1) to monitor the transverse profile, pointing and charge of the electron bunch. Absolute charge calibration has been conducted using imaging plates (Paterson et al. 2008). To transport the beam, a compact triplet of permanent magnetic quadrupoles (PMQs) can be placed 2 cm after the accelerator (Eichner et al. 2007). The quadrupoles are designed to transport a wide energy range of mono-energetic electron bunches. Here, they are optimized for 130 MeV mono-energetic electron beams in combination with a triplet of electromagnetic quadrupoles (EMQs) placed 1 m further downstream. Varying the separation of the PMQ triplet components allows successful transport of a wide energy range electron beams over the entire length of the beam line.

To characterize the electron energy spectrum, the ALPHA-X imaging dipole magnet electron spectrometer is utilized. Placed 2.5 m after the accelerator, it has the capability of measuring electron energies up to ~660 MeV. The spectrometer features a Browne–Buechner design (Browne and Buechner 1956) to provide strong focusing in both the horizontal and vertical planes, thus, enabling excellent energy resolution to be maintained over the wide energy range (from <1% at the lower end to ~10% at the upper end). Measurements are performed in a high energy measurement regime where a high magnetic field ~0.5 T is applied. Scintillating Ce:YAG crystals are placed at the image plane of the spectrometer and imaged using a high resolution CCD camera.

Transverse emittance measurements are performed using the pepper-pot technique (Yamazaki et al. 1992). A 125 μm thick tungsten mask with a 27 × 27 array of 25 μm diameter holes with a period of 150 μm is used to intercept the electron bunch 30 cm after the accelerator thereby producing an array of electron beamlets superimposed on a smoothly varying background. Simulations using GEANT4 (Agostinelli et al. 2003) have been performed to verify that this method would provide accurate emittance measurements for this beam energy. These electron beamlets are measured 60 cm downstream on a thin Ce:YAG crystal which is isolated from any stray light.

## 3. Experimental results

As shown in Fig. 2, narrow energy spread bunches have been obtained using the ALPHA-X electron spectrometer (E-SPEC) operating in its high energy configuration where, at electron energies above ~100 MeV, optimal focussing of the beam in the imaging plane of the spectrometer can be obtained with additional beam collimation provided by the EMQs (no PMQs have been used for these measurements). The dependence of the spectrometer response on the electron beam properties is well understood from General Particle Tracer (GPT) (van der Geer et al. 2005) simulations and estimations of the detection system resolution are consistent with the narrowest measured energy spreads (Wiggins et al. 2009). For the energy range discussed here, the resolution is typically 0.3–1.0%.

Due to the design of our nozzle, and with fixed laser parameters, the electron energy can be tuned over a wide energy range (90–220 MeV) and the measured r.m.s. relative energy spread of the main bunch is as

https://doi.org/10.1017/S0022377812000220 Published online by Cambridge University Press

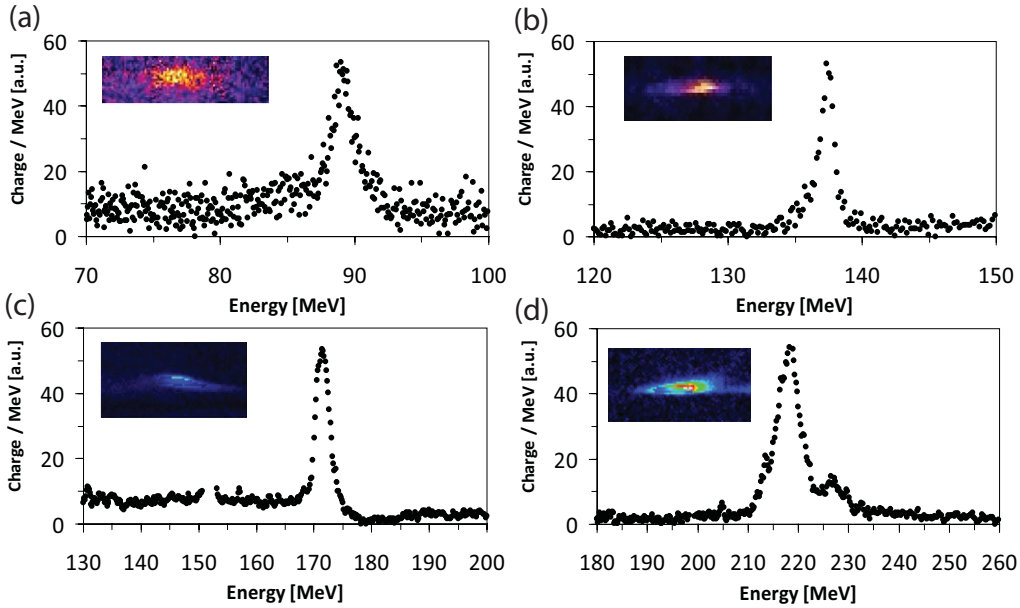


**Figure 2.** (Colour online) Electron energy spectra with false colour YAG screen images inset: (a) 89 MeV, 0.8% spread bunch measured with EMQs: $Q1 = 47$ mT, $Q2 = 22$ mT, $Q3 = 0$ and E-SPEC: 0.59 T. (b) 137 MeV, 0.5% spread bunch measured with EMQs: $Q1 = 62$ mT, $Q2 = 65$ mT, Q3 = 72 mT and E-SPEC: 0.43 T. (c) 171 MeV, 0.7% spread bunch measured with EMQs: $Q1 = 55$ mT, $Q2 = 55$ mT, $Q3 = 51$ mT and E-SPEC: 0.56 T. (d) 218 MeV, 1.1% spread bunch measured with EMQs: $Q1 = 82$ mT, $Q2 = 76$ mT, $Q3 = 81$ mT and E-SPEC: 0.74 T.

low as 0.5% (Fig. 2(b)). Convolution by the detection system response implies an actual energy spread as low as ~0.3%. In each case, the bunch charge is low (~0.5 – 1.0 pC) ensuring that the self-injection process is close to threshold such that the phase-space volume for injection is small and the resultant emittances are low. The r.m.s spread has been calculated solely for the main electron energy peak, i.e. the background is neglected, with a Gaussian profile fitted to each peak. This approach is justified from the viewpoint of FEL radiation generation that is determined by the properties of the main bunch only. For other applications, the entire electron beam may have to be accounted for and, in this case, the r.m.s energy spread is larger (but still 1–2% in the best shots). Energy tunability is mainly determined by the reciprocal scaling with plasma density (Lu et al. 2007). At higher plasma density $\sim 3.2 \times 10^{19} \mathrm{cm}^{-3}$, the central electron energy of the bunch decreases to around 90 MeV (Fig. 2(a)) while, at lower density $\sim 1.3 \times 10^{19}\,\mathrm{cm}^{-3}$, the central electron energy has reached as high as 218 MeV (Fig. 2(d)). At these plasma densities, the laser $a_0$ parameter is indicated to increase to ~2.4, which is close to that expected because of self-focusing and photon acceleration effects (Reitsma et al. 2005).

Figure 3(a) shows an electron beam measured 60 cm after the accelerator. Here a thin Ce:YAG crystal, which has higher spatial resolution (10 μm) than Lanex (>100 μm), is used for imaging during the emittance measurement. The pepper-pot mask is introduced into the beam axis using a motorized rotation stage. Both the laser and the electron beam travel through the mask before being blocked by an aluminium foil at the detection crystal. The GPT calculations have shown that by allowing the electron beam to travel through the laser blocking foil placed as close as possible to the detector any degradation of the emittance measurement is minimized (Manahan et al. 2011). A typical beamlets recorded image is shown in Fig. 3(b) and, by analysing consecutive shots, a distribution of emittance has been determined. A mean value of $2.2 \pm 0.7$ π-mm-mrad is obtained for the horizontal emittance with best value of $1.1 \pm 0.1$ π-mm-mrad. For vertical emittance, a mean value of $2.3 \pm 0.6$ π-mm-mrad is obtained and with a best emittance of $1.2 \pm 0.1$ π-mm-mrad (Brunetti et al. 2010; Manahan et al. 2011).

Simultaneous pepper-pot and electron spectrometer measurements are not possible, thus, the average electron energy in the emittance experimental run has been determined immediately afterwards upon removal of the mask and imaging crystal from the beam line axis. A sequence of 200 consecutive shots resulted in an average central energy for the main bunch of $125 \pm 3$ MeV, which demonstrates the stability of the accelerator and is consistent with other measurements (Wiggins et al. 2010). The ellipticity evident in the transverse beam profile (aspect ratio = 1.05) is reproduced in the emittance calculation. The transverse emittances obtained are comparable with conventional linear accelerators (Carneiro et al. 1999), yet the lowest measured values along the horizontal and vertical directions still represent an upper limit because of the resolution limit of the detection system. Future upgrades for this single-shot diagnostic will entail refinement of the mask geometry, imaging screen spatial resolution and drift distance between mask

https://doi.org/10.1017/S0022377812000220 Published online by Cambridge University Press

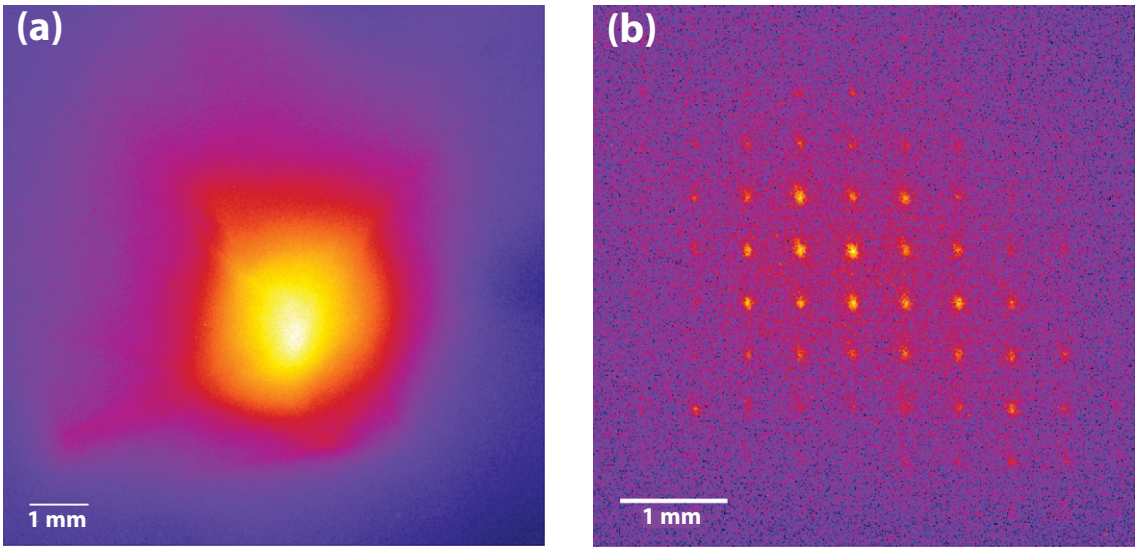


**Figure 3.** (Colour online) (a) False-colour image of an electron beam without the mask measured on a YAG crystal. (b) Electron beamlets produced after propagating through the pepper-pot mask.

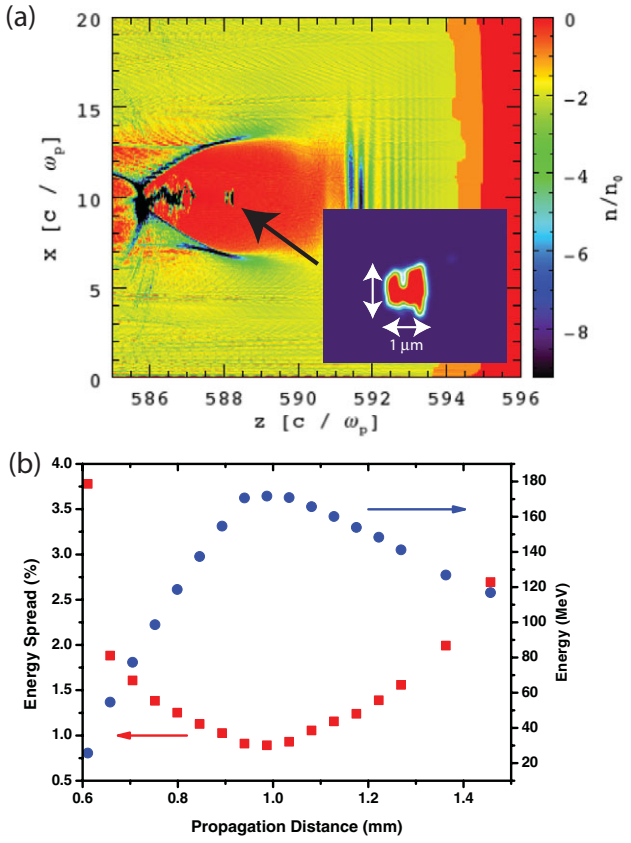


**Figure 4.** (Colour online) OSIRIS simulation of the accelerator: (a) electron density distribution after 0.99 mm of propagation (a magnified surface plot is displayed in the inset) and (b) evolution of central energy and energy spread with propagation distance. Plasma density = $1.0 \times 10^{19}$ cm$^{-3}$, laser vector potential = 1.6, initial pulse duration = 35 fs and initial spot size = 20 μm. Electron bunch charge is 3 pC.

and imaging screen. Applicability up to an electron energy of 300 MeV should be achievable with an increased mask thickness of 250 μm.

Comparable high quality electron beams (spread <1%, transverse emittance <1 $\pi$-mm-mrad) can be generated in 3-D particle-in-cell (PIC) simulations, as shown in Fig. 4. These simulations have been performed using the OSIRIS code (Fonseca et al. 2002) with the number of cells set as (1500:300:300) in a box of (12:20:20) $(c/\omega_p)^3$, where $c$ is the speed of light in vacuum and the propagation direction is along $+z$-axis. The energy spread is seen to reach a minimum of 0.8% at the dephasing point (1 mm of propagation) where the energy reaches a maximum of 170 MeV but it remains an open issue to fully reconcile the simulation results with experimental observations. Most significantly, an initial laser $a_0$ value of 1.6 has been used in simulations to obtain such bunches (initiate self-injection) which, clearly, is significantly higher than the initial $a_0$ applied experimentally (1.0). On-going studies are concerned with the gas jet nozzle behaviour and plasma channel formation and initial results indicate a high sensitivity to the entrance plasma density ramp that is of length 140 μm in the PIC simulation of Fig. 4 but may be much longer in experiments (unpublished). In agreement with experiment, high quality bunch parameters are coupled to low charge injection (~3 pC in the simulation, contained in a 1 μm$^3$ volume) so high sensitivity to accelerator conditions are expected when operating close to the injection threshold.

Figure 5(a) shows an averaged image of 200 consistent laser-induced plasma channels produced across the gas jet with the onset of the channel several 100s of μm before the nozzle location indicating a long entrance density ramp. The dashed circle represents the inner wall of the nozzle and is 2 mm in diameter. The laser propagates 2.3 mm above the exit of the nozzle and the backing pressure of the helium gas was 30 Bar. The plasma channel length here is ~2 mm, consistent with other observations (Huntington et al. 2011). Based on

https://doi.org/10.1017/S0022377812000220 Published online by Cambridge University Press

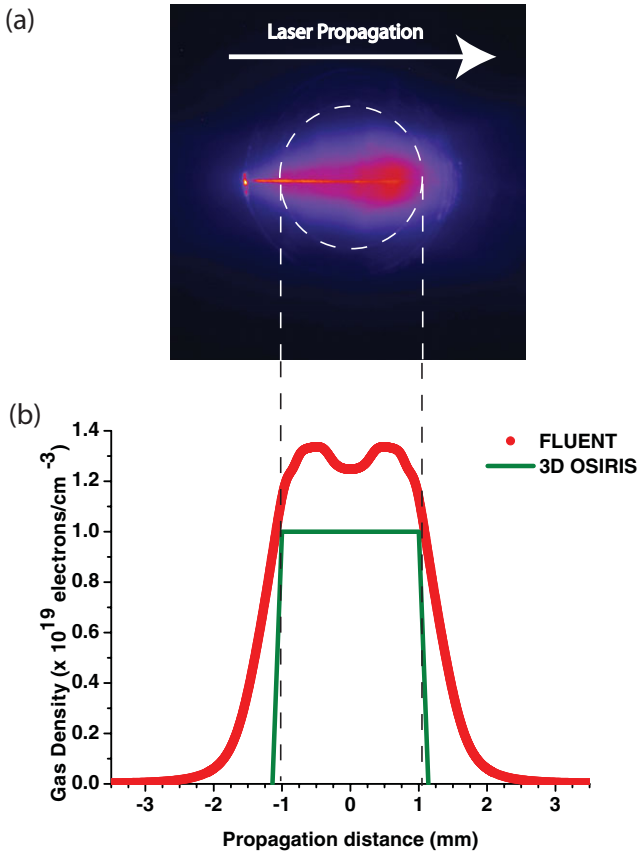


**Figure 5.** (Colour online) (a) Top–down, false colour image of laser channel produced 2.3 mm above the gas nozzle. The laser is focussed to $\omega_0 = 40\,\mu$m in 30 Bar backing pressure of He gas. The image represents the average of 200 consecutive images. (b) FLUENT simulation results of the gas density profile at 2.3 mm above the nozzle for 30 Bar backing pressure for the supersonic gas nozzle used in experiments. Also shown is the gas density profile and density ramp assumed for 3-D OSIRIS simulations.

this, our approach to study the density ramp has been to carefully simulate the expected density profile from our supersonic nozzle.

Gas flow simulations have been performed using the commercial software ANSYS®FLUENT 6.3.26 and the modelling and meshing of the nozzle is included using GAMBIT 2.4.6. The model used for the simulation is a SST $k$-$\omega$ turbulence model suitable for our gas nozzle and flow (Schmid 2009). The density-based coupled implicit solver is used as is standard for supersonic flows. Due to large variations in all flow parameters, a double precision solver is utilized. The gas nozzle is set in a 2-D axis symmetric geometry, where the mesh size is set to resolve all characteristics of the flow, the most important being turbulences. A boundary layer consisting of 30 rows of cells, 16.4 μm thick, has been used for the walls of the nozzle. This enables the gas flow to be resolved since it reduces by 90% close to the gas wall and ultimately affects the density gradient width. The total number of cells used for this simulation is 1 078 800. All simulations use helium gas at a backing pressure of 30 Bar, temperature of 300 K and the gas density profile was calculated at 2.3 mm above the nozzle exit, as shown in Fig. 5(b). FLUENT simulations assume continuous flow which, due the long opening time (2.5 ms) of the gas valve in the experiment, is a valid assumption. Also, the gas density calculated (and the plasma density used for 3-D OSIRIS simulations) assumes 100% ionization of the gas.

Figure 5(b) shows the gas density profile calculated from FLUENT simulations and also the assumed profile used in 3-D OSIRIS simulations (Fig. 4). The FLUENT simulation shows long density rising and falling ramps with a maximum gas density of $\sim 1.3 \times 10^{19}$ electrons/cm$^{-3}$. The oscillation evident in the profile is due to shocks generated from the nozzle. These shocks are both dependant on the backing pressure used and the distance above the nozzle exit. Evidently, the profile used for OSIRIS simulations is significantly different and will require further investigation to produce conditions matching that applied in the experiments. The inclusion of shocks and investigation of the range of peak densities applied experimentally will be the subject of a separate publication. Currently, an *in-situ* interferometer is being installed at the LWFA gas nozzle to verify the plasma density profile. To date, off-line characterization of the nozzle has been used to obtain plasma density information.

## 4. Summary

We have presented a review of the achievable electron beam on the ALPHA-X beam line. Measurements of the electron energy have shown that stable, monoenergetic electron bunches are produced with measured r.m.s. energy spread down to $\sigma_\gamma/\gamma = 0.5\%$. Moreover, emittance measurements have shown that the measured emittance, $1.1 \pm 0.1$ $\pi$-mm-mrad, is comparable to that of conventional accelerators. Properties such as these, coupled with the lower cost and significant reduction in size, emphasize the LWFA as a strong competitor in the advancing field of accelerator technology. The ALPHA-X laser–plasma accelerator emphasizes the application possibilities, such as driving a compact table-top FEL, from a tenable high quality source.

The PIC simulations of our accelerator give further insight into the production of high quality electron beams with low charge. Maintaining a bunch length of $\sim 1\,\mu$m along the beam line would represent a peak current of $\sim 1$ kA, suitable for FEL application. Gas flow simulations and improved accelerator diagnostics are being implemented to fully understand experimental conditions (including density shocks and ramps) which may lead to fully consistent replication of experimental electron beam generation in PIC simulations.

## Acknowledgements

We acknowledge the support of the U.K. EPSRC, the EC's Seventh Framework Programme (LASERLAB-EUROPE/LAPTECH, grant agreement no. 228334) and

https://doi.org/10.1017/S0022377812000220 Published online by Cambridge University Press

the Extreme Light Infrastructure (ELI) European Project. We thank T. McCanny and D. Clark for technical support and K. Schmid for technical discussions.

## References

Agostinelli, S., Allison, J., Amako, K., Apostolakis, J., Araujo, H., Arce, P., Asai, M., Axen, D., Banerjee, S. et al. 2003 GEANT4-a simulation toolkit. *Nucl. Instrum. Methods Phys. Res. A – Accel. Spectrom. Detect. Assoc. Equip.* **506**, 250–303.

Browne, C. P. and Buechner, W. W. 1956 Broad-range magnetic spectrograph. *Rev. Sci. Instrum.* **27**, 899–907.

Brunetti, E., Shanks, R. P., Manahan, G. G., Islam, M. R., Ersfeld, B., Anania, M. P., Cipiccia, S., Issac, R. C., Raj, G. et al. 2010 Low emittance, high brilliance relativistic electron beams from a laser-plasma accelerator. *Phys. Rev. Lett.* **105**, 215 007.

Carneiro, J. P., Carrigan, R. A., Champion, M. S., Colestock, P. L., Edwards, H. T., Fuerst, J. D., Hartung, W. H., Koepke, K. P., Kuchnir, M. et al. 1999 In *Proc. Invited Papers, 18th Biennial Particle Accelerator Conference*, Vol. 3, (Eds. A. Luccio and W. MacKay). Institute of Electrical and Electronics Engineers, New York, 1999, New York City, pp. 2027–2029.

Cipiccia, S., Islam, M. R., Ersfeld, B., Shanks, R. P., Brunetti, E., Vieux, G., Yang, X., Issac, R. C., Wiggins, S. M. et al. 2011 Gamma-rays from harmonically resonant betatron oscillations in a plasma wake. *Nat. Phys.* **7**, 867.

Eichner, T., Gruner, F., Becker, S., Fuchs, M., Habs, D., Weingartner, R., Schramm, U., Backe, H., Kunz, P. et al. 2007 Miniature magnetic devices for laser-based, table-top free-electron lasers. *Phys. Rev. Spec. Topics – Accel. Beams* **10**, 9.

Faure, J., Rechatin, C., Norlin, A., Lifschitz, A., Glinec, Y. and Malka, V. 2006 Controlled injection and acceleration of electrons in plasma wakefields by colliding laser pulses. *Nature* **444**, 737–739.

Fonseca, R. A., Silva, L. O., Tsung, F. S., Decyk, V. K., Lu, W., Ren, C., Mori, W. B., Deng, S., Lee, S. et al. 2002 OSIRIS: a three-dimensional, fully relativistic particle in cell code for modeling plasma based accelerators. In: *Proc. Comput. Sci.-Iccs 2002, Pt Iii,* Vol. 2331 (ed. P. Sloot, C. J. K. Tan, J. J. Dongarra and A. G. Hoekstra). Berlin: Springer-Verlag Berlin, pp. 342–351.

Fritzler, S., Lefebvre, E., Malka, V., Burgy, F., Dangor, A. E., Krushelnick, K., Mangles, S. P. D., Najmudin, Z., Rousseau, J. P. et al. 2004 Emittance measurements of a laser-wakefield-accelerated electron beam. *Phys. Rev. Lett.* **92**, 4.

Fuchs, M., Weingartner, R., Popp, A., Major, Z., Becker, S., Osterhoff, J., Cortrie, I., Zeitler, B., Horlein, R. et al. 2009 Laser-driven soft-X-ray undulator source. *Nat. Phys.* **5**, 826–829.

Huntington, C. M., Thomas, A. G. R., McGuffey, C., Matsuoka, T., Chvykov, V., Kalintchenko, G., Kneip, S., Najmudin, Z., Palmer, C. et al. 2011 Current filamentation instability in laser wakefield accelerators. *Phys. Rev. Lett.* **106**, 4.

Jaroszynski, D. A., Bingham, R., Brunetti, E., Ersfeld, B., Gallacher, J., van der Geer, B., Issac, R., Jamison, S. P., Jones, D. et al. 2006 Radiation sources based on laser-plasma interactions. *Phil. Trans. R. Soc. A – Math. Phys. Eng. Sci.* **364**, 689–710.

Leemans, W. P., Nagler, B., Gonsalves, A. J., Toth, C., Nakamura, K., Geddes, C. G. R., Esarey, E., Schroeder, C. B. and Hooker, S. M. 2006 GeV electron beams from a centimetre-scale accelerator. *Nat. Phys.* **2**, 696–699.

Lu, W., Tzoufras, M., Joshi, C., Tsung, F. S., Mori, W. B., Vieira, J., Fonseca, R. A. and Silva, L. O. 2007 Generating multi-GeV electron bunches using single stage laser wakefield acceleration in a 3D nonlinear regime. *Phys. Rev. Spec. Topics – Accel. Beams* **10**, 12.

Lundh, O., Lim, J., Rechatin, C., Ammoura, L., Ben-Ismail, A., Davoine, X., Gallot, G., Goddet, J. P., Lefebvre, E. et al. 2011 Few femtosecond, few kiloampere electron bunch produced by a laser-plasma accelerator. *Nat. Phys.* **7**, 219–222.

Manahan, G. G., Brunetti, E., Shanks, R. P., Islam, M. R., Ersfeld, B., Anania, M. P., Cipiccia, S., Issac, R. C., Raj, G. et al. 2011 High resolution, single shot emittance measurement of relativistic electrons from laser-driven accelerator. In: *Laser Acceleration of Electrons, Protons, and Ions and Medical Applications of Laser-Generated Secondary Sources of Radiation and Particles*, Vol. 8079 (ed. W. P. Leemans, E. Esarey, S. M. Hooker, K. W. D. Ledingham, K. Spohr and P. McKenna). Bellingham: Spie-Int Soc Optical Engineering, p. 807 909.

Mangles, S. P. D., Murphy, C. D., Najmudin, Z., Thomas, A. G. R., Collier, J. L., Dangor, A. E., Divall, E. J., Foster, P. S., Gallacher, J. G. et al. 2004 Monoenergetic beams of relativistic electrons from intense laser-plasma interactions. *Nature* **431,** 535–538.

Paterson, I. J., Clarke, R. J., Woolsey, N. C. and Gregori, G. 2008 Image plate response for conditions relevant to laser – plasma interaction experiments. *Meas. Sci. Technol.* **19**, 095 301.

Rechatin, C., Faure, J., Ben-Ismail, A., Lim, J., Fitour, R., Specka, A., Videau, H., Tafzi, A., Burgy, F. and Malka, V. (2009) Controlling the Phase-Space Volume of Injected Electrons in a Laser-Plasma Accelerator. *Phys. Rev. Lett.* **102**, 4.

Reitsma, A. J. W., Cairns, R. A., Bingham, R. and Jaroszynski, D. A. 2005 Efficiency and energy spread in laser-wakefield acceleration. *Phys. Rev. Lett.* **94**, 085 004.

Rousse, A., Phuoc, K. T., Shah, R., Pukhov, A., Lefebvre, E., Malka, V., Kiselev, S., Burgy, F., Rousseau, J. P. et al. 2004 Production of a keV x-ray beam from synchrotron radiation in relativistic laser-plasma interaction. *Phys. Rev. Lett.* **93**, 4.

Schlenvoigt, H. P., Haupt, K., Debus, A., Budde, F., Jackel, O., Pfotenhauer, S., Schwoerer, H., Rohwer, E., Gallacher, J. G. et al. 2008 A compact synchrotron radiation source driven by a laser-plasma wakefield accelerator. *Nat. Phys.* **4**, 130–133.

Schmid, K. 2009 *Supersonic Micro-Jets and Their Application to Few Cycle Laser Driven Electron Acceleration.* München: LMU.

Sears, C. M. S., Buck, A., Schmid, K., Mikhailova, J., Krausz, F. and Veisz, L. 2010 Emittance and divergence of laser wakefield accelerated electrons. *Phys. Rev. Spec. Topics – Accel. Beams* **13**, 092 803.

Sprangle, P., Esarey, E. and Ting, A. 1990 Nonlinear-interaction of intense laser-pulses in plasmas. *Phys. Rev.* A **41**, 4463–4467.

Sun, G. Z., Ott, E., Lee, Y. C. and Guzdar, P. 1987 Self-focusing of short intense pulse in plasmas. *Phys. Fluids* **30**, 526–532.

Tajima, T. and Dawson, J. M. 1979 Laser electron-accelerator. *Phys. Rev. Lett.* **43**, 267–270.

van der Geer, S. B., Luiten, O. J., de Loos, M. J., Poplau, G. and van Rienen, U. 2005 3D space-charge model for GPT simulations of high-brightness electron bunches. In: *Computational Accelerator Physics 2002*, Vol. 175 (ed. M. Berz and K. Makino). Bristol: IOP Publishing Ltd, pp. 101–110.

Wiggins, S. M., Anania, M. P., Brunetti, E., Cipiccia, S., Ersfeld, B., Islam, M. R., Issac, R. C., Raj, G., Shanks, R. P. et al. 2009 Narrow spread electron beams from a laser-plasma wakefield accelerator. In: *Harnessing Relativistic Plasma Waves as Novel Radiation Sources from Terahertz to X-Rays and Beyond*, Vol. 7359 (ed. D. A. Jaroszynski and A. Rousse) Bellingham: Spie-Int Soc Optical Engineering, pp. 735 914.

Wiggins, S. M., Issac, R. C., Welsh, G. H., Brunetti, E., Shanks, R. P., Anania, M. P., Cipiccia, S., Manahan, G. G., Aniculaesei, C. et al. 2010 High quality electron beams from a laser wakefield accelerator. *Plasma Phys. Control. Fusion* **52**, 124 032.

Yamazaki, Y., Kurihara, T., Kobayashi, H., Sato, I. and Asami, A. 1992 High-precision pepper-pot technique for a low-emittance electron-beam. *Nucl. Instrum. Methods Phys. Res. A – Accel. Spectrom. Detect. Assoc. Equip.* **322**, 139–145.

https://doi.org/10.1017/S0022377812000220 Published online by Cambridge University Press